Three-Dimensional Microstructural Measurement for Predicting the Risk of Osteoporotic Fracture

Nobuhito Nango, Shogo Kubota, and Yusuke Horiguchi

Keywords

Four-dimensional quantitative computed tomography (4DQCT) · 3D bone morphometry · Vertebral fracture · 3D star volume · Therapeutic effects on osteoporosis

1 Introduction

More than half of women older than 50 years and men older than 70 years are at risk for fracture because of osteoporosis, and prevention of fracture is a global issue [1].

Bone mineral density (BMD) is currently used to diagnose osteoporosis measured by dual-energy X-ray absorptiometry (DXA). However, in some cases, the risk of fracture is high even if the BMD is high. In 2001, the National Institutes of Health (NIH) of the United States released a description of bone quality in addition to BMD as a factor that influences bone strength [1]. "Bone density accounts for almost 70% of bone strength, and the remaining 30% can be explained by bone quality. It is microstructure, bone turnover, microfractures, and mineralization of bone tissue that define bone quality." In this report, the importance of bone quality in bone fracture prevention was recognized.

Bisphosphonates, a class of bone resorption inhibitor, suppress bone resorption and reduce remodeling. They are also demonstrated to prevent fractures. However, new side effects have been reported due to the accumulation of therapeutic results of bone resorption inhibitors. The US Food and Drug Administration (FDA) warned that

N. Nango (✉) · S. Kubota · Y. Horiguchi
Ratoc System Engineering Co., Ltd, Tokyo, Japan
e-mail: nango@ratoc.co.jp

long-term use entails a risk of atypical femoral fractures [2]. Prolonged administration of bisphosphonates has been cited as carrying potential risks of bone deterioration, suppression of bone formation, homogeneous calcification of the bone unit, excessive calcification, hardness and brittleness of bones, and accumulation of microcracks [3].

Degradation and aging of bone material have been noted, and the importance of the balance between absorption and formation that modifies bone material has been recognized.

Conventionally, bone microstructure, bone resorption, and the amount of bone formation have been measured by histomorphometry. Histomorphometry is advantageous as it can directly measure cell activity. However, the measurement site is limited because it is invasive, and it is a two-dimensional measurement. On the other hand, an X-ray CT image is also advantageous as it is less invasive and can image calcified bones of the entire body in three dimensions (3D).

3D bone morphometry can be used to measure bone mineralization, bone mass, size, connectivity, and shape using computed tomographic (CT) images, thereby quantifying the risk of fracture. It is not possible to measure the presence of cells directly. An hydroxyapatite (HA) phantom is scanned at the same time during X-ray CT imaging to obtain a bone mineralization image. From the 3D images, it is possible to characterize the skeletal strength and vulnerabilities throughout the body.

The fracture risk is quantified by bone structure, degree of bone mineralization, and simulation, and the current bone fragility is quantified. The goal is to be able to predict and evaluate the effect of medication that considers the balance between bone mass, bone quality, and remodeling and can also consider the fracture risk of individual patients.

2 Mechanism of Vertebral Fracture in Osteoporosis

2.1 Porosity in the Vertebral Cancellous Bone

Advancing osteoporosis and loss of cancellous bone increase the risk of vertebral fracture. Using the first lumbar vertebra (L1), which is at high risk of fracture, as an example, we examined the fragility of the cancellous bone that leads to vertebral body fracture due to porosity (Fig. 1). Multidetector computed tomographic (MDCT) images were obtained and examined in cases with different fracture risk stages. The gray scale indicates the degree of calcification. The center image in Fig. 1 is a 3-mm thick horizontal cross section of the center of the vertebral body, the right image is a 3-mm-thick sagittal cross section of the vertebral body, and the left image is a schematic diagram of the cancellous bone. In a healthy 68-year-old man (Fig. 1a), the degree of calcification in the cortical shell was higher than that of the internal cancellous bone, and the cortical shell was thick. The horizontal section showed that the cancellous bone inside the cortical shell was concentrically connected with beams in layers parallel to the contour. The beams extended radially in the front–back direction. The sagittal image shows that the cancellous bone extended vertically, supporting the end plate, and was dense. The inferior end plate had multiple beams extending in parallel in the anterior–posterior direction. A healthy
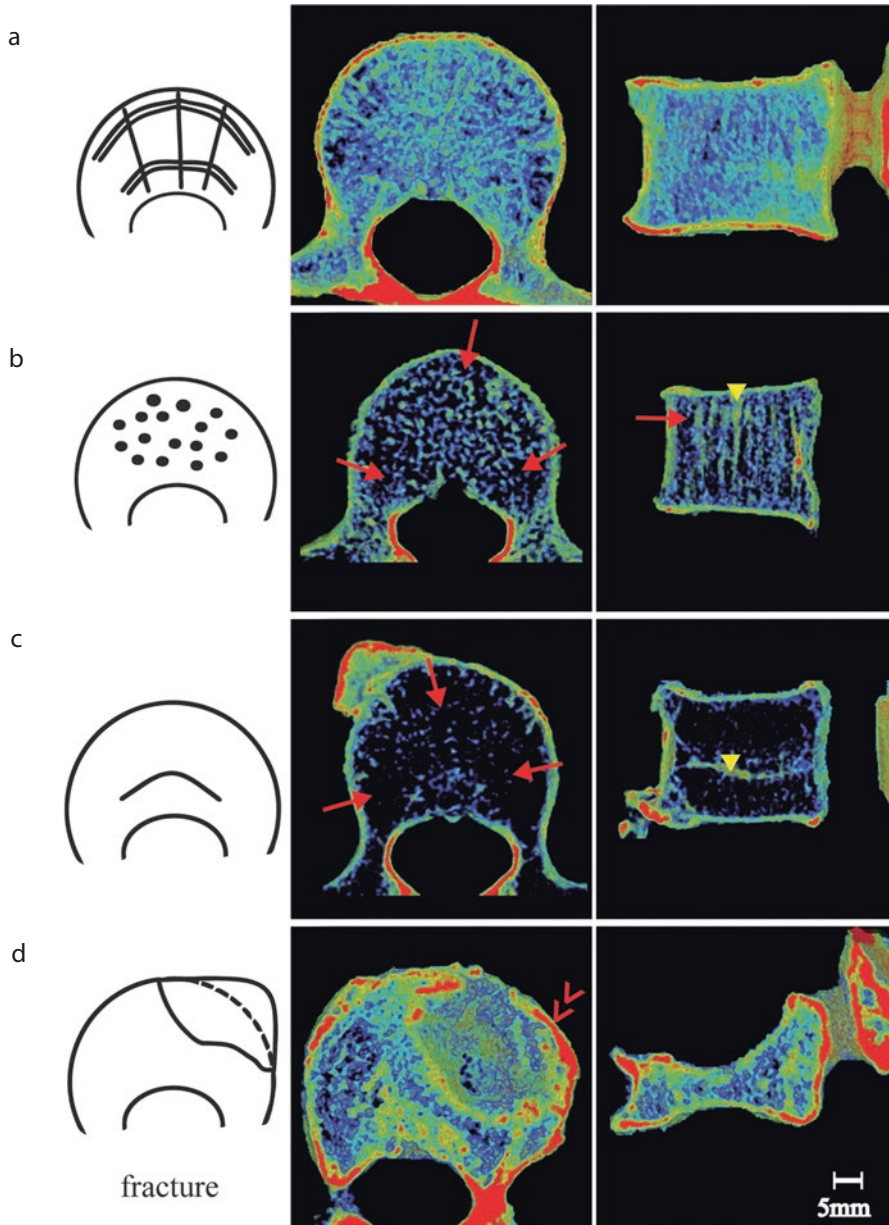
Fig. 1 Loss of cancellous bone increases the risk of vertebral fracture. (**a**) A healthy 68-year-old man, a honeycomb structure composed of bone plates. (**b**) A 63-year-old woman with moderate osteoporosis, the bone marrow expanded (→). (**c**) An 82-year-old woman with severe osteoporosis, the cortical shell bore the weight. (**d**) An 80-year-old woman with a fracture of L1, depression of the end plate. →: bone marrow cavity. △: thickened trabeculae. >>: popped out endplate

vertebral cancellous bone was mainly composed of plate-shaped bones and had a honeycomb structure in the anterior–posterior, lateral, and superior–inferior directions.

In a 63-year-old woman with moderate osteoporosis (Fig. 1b), dots representing bone loss were scattered throughout the specimen, which show the cancellous bone extended in the vertical direction. Both the cancellous bone in the anterior–posterior and lateral directions and the honeycomb-like structure were lost. In the cancellous bone near the cortical shell, the connection with the cortical shell was remarkably reduced in comparison with the normal appearance. The cancellous bone near the anterior and lateral sides disappeared, and the bone marrow cavity, which does not support the load, expanded (→). On the other hand, as shown in the sagittal image, thick cancellous bones that connected the upper and lower end plates were present at the center of the vertebral body. It was composed of thick, rod-shaped cancellous bone, although its density was low (△). The vertical load was also supported by the cancellous bone.

In an 82-year-old woman with severe osteoporosis (Fig. 1c), the cancellous bone inside the vertebral body almost disappeared, and several thick trabeculae barely extended in the anterior–posterior direction at the center of the vertebral body, supporting the anterior–posterior direction of the cortical shell. The cortical shell carried the load. The cancellous bone that supported the cortical shell from the inside disappeared. Therefore, it could be expected that the cortical shell is deformed by the load applied to the body, which indicates that the risk of fracture was high.

In an 80-year-old woman with an L1 fracture (Fig. 1d), the right front part of the vertebral body fractured and collapsed. The image on the right shows that the cortical shell at the center bent outward with the lower part as a fulcrum, and the cortex protruded from its original position (>>). The end plate was also torn off. The cancellous bone folded and overlapped, giving the cancellous bone a denser appearance.

When a fracture of a vertebral body is left untreated, it is crushed until the upper and lower end plates overlap and form a plate shape, and then, it stabilizes.

2.2   Aging-Related Changes in Bone Structure

A bone is a metabolizing organ, and its resorption and formation are continuous processes. Osteoclasts resorb bone, osteoblasts form bone, and osteocytes maintain bone. A bone is characterized by its ability to be restored to its original shape after a fracture. After adolescence, bones finish growth and achieve maximum mass (peak bone mass) by the middle of the third decade. After that, although remodeling continues, the maximum bone mass gradually decreases, but the same structure is maintained for a long time.

2.3   Osteoporosis

Bone resorption and bone formation take place continuously. In adults, approximately 300 mg of calcium passes in and out of bone daily. The immediate response to a decrease in blood calcium concentration is bone resorption. After bone resorption, a delay in bone formation automatically causes a reduction in bone mass. Older people have increased bone turnover, and before the bone resorption surface is repaired, new resorption begins; without interventions such as medication, the bone mass decreases. Bones support a person's total weight, and they bear more than 5 times their own weight to move and 10 times the load when the person falls. Thus, elderly people with osteoporosis are at risk of fractures [4].

In a cancellous bone with osteoporosis, remodeling is more active than in cortical bone, and when bone resorption is increased, the continuity and connectivity of cancellous bone are disrupted and the trabeculae may disappear. Loss of cancellous bone also leads to loss of the beams that connect to the cortical bone, which increases the strain on the cortical bone and increases the risk of fracture. Resorption of the endosteum is enhanced in the cortical bone as tunnel-like structures penetrate the cortex. Cortical bone has increased voids, which thins the cortical shell and eventually becomes cancellous.

Figure 2 shows cancellous bone thickness of the vertebral body in pseudo-color. Thick cancellous bone is indicated in yellow and thin cancellous bone in blue.
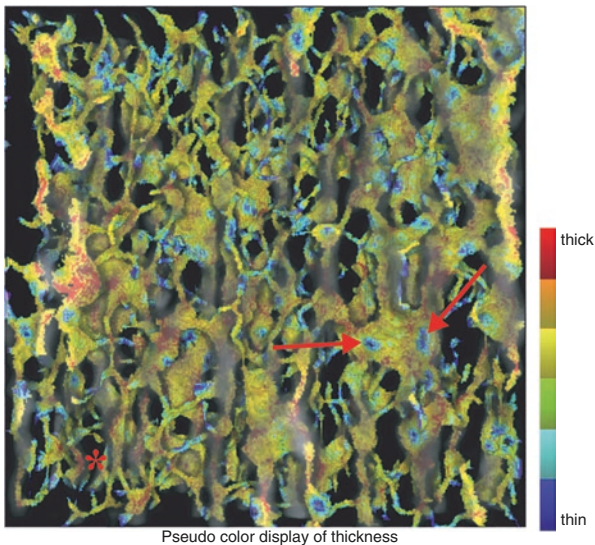

Pseudo color display of thickness

Fig. 2 Cancellous bone thickness of a vertebral body affected by osteoporosis. →: Perforation. *: Cavity. The vertical body is a mixture of plate-shaped bone (yellow), thinning trabeculae (green), perforations (blue), rod-shaped bone (narrow), and cavities (black, around rod-shaped bone)

Fig. 3 X-ray CT image of an iliac biopsy sample with osteoporosis. A large resorption cavity in the cortical bone on the right side, and conversion of the cortical bone to the shape of cancellous bone is progressing ($\rightarrow$). *: Defect. △: Perforation. $\rightarrow$: Trabecularized cortex
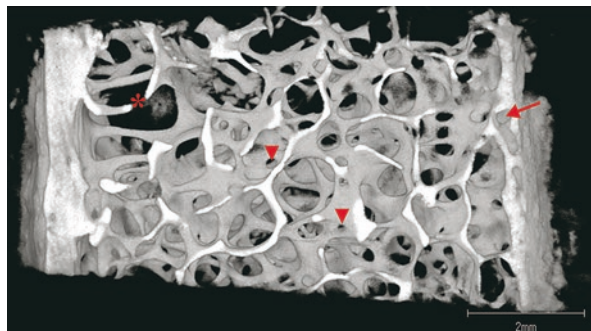
The wide part indicates the plate bone. Red indicates thick plate bone, and yellow and green indicate thin plate bones. There are many blue dots on the plate bone ($\rightarrow$). The part with a black dot in the center of the blue dot indicates the presence of perforation. The size of the holes in the perforation ranges from small to large, indicating that the holes expand. Some rod-shaped bones are indicated by a blue line and are at a risk of loss. The cavity was expanded around the rod-shaped bone (*), and osteoporosis was locally enhanced. Figure 3 shows cortical bone with osteoporosis. This is a µCT image of an iliac biopsy sample from a patient with osteoporosis. The left and right ends of the bone are the cortical bone, and the middle is the cancellous bone. Perforation of plate-like cancellous bone and rod-like trabeculae are present everywhere (△). On the upper side of the image, the cancellous bone appears rod-shaped and the defect (*) spreads. The thickness of the cortical bone on the right side is less than half that of the cortical bone on the left side. A large resorption cavity in the cortical bone on the right side has caused loss of the cortical bone, and conversion of the cortical bone to the shape of cancellous bone is progressing ($\rightarrow$).

2.4   Mechanism of Vertebral Body Fracture

We investigated the mechanism of vertebral body compression fracture under the assumption that the deterioration of the cancellous bone was caused by increased bone resorption (Fig. 4). A healthy vertebral cancellous bone is mainly plate shaped; it has beams extending in the loading direction, the anterior–posterior direction, and the lateral direction; and it has a honeycomb-like, mechanically strong structure (Fig. 4a). As osteoporosis progresses in the cancellous bone, resorption becomes more common than bone formation, and the plate-shaped bone is absorbed and thinned at the center (Fig. 4b) and eventually becomes perforated and rod shaped (Fig. 4c). The ability of the cancellous bone to withstand stress also changes. Resorption occurs in the low-stress area that does not support the load, and the cancellous bone ruptures (Fig. 4d). The involved trabecular bone is resorbed and disappears because it does not support the load (Fig. 4e). The disappearance of the cancellous bone enlarges locally, forming a cavity (Fig. 4f*). The surrounding
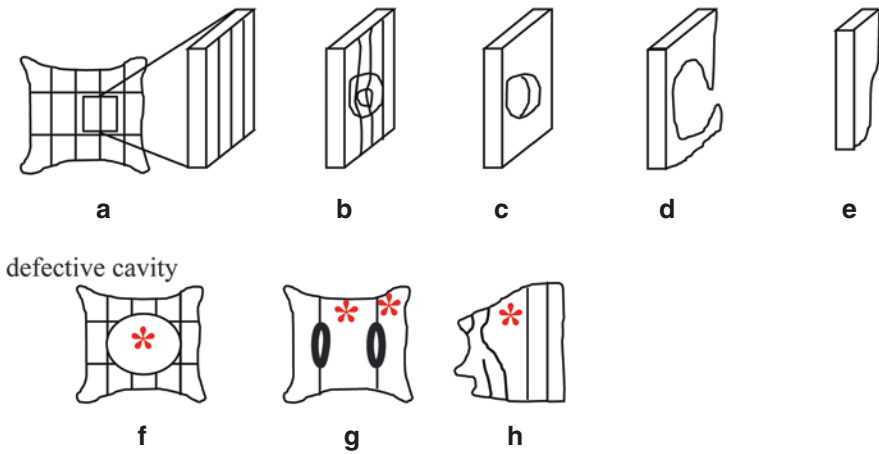
Fig. 4 Mechanism of compression fracture of a vertebral body. In a healthy person, the bone has a honeycomb structure (**a**). Osteoporosis progresses and bone undergoes resorption in the center (**b**) and thinned trabeculae become perforated rod-shaped bone (**c**). The cancellous bone breaks (**d**) and the trabeculae are resorbed and disappear (**e**). The missing cancellous bone enlarges the locally defective cavity (*) (**f**). The surrounding cancellous bone increases both the strain and the risk of cancellous bone fracture (**g**). The beam that supports the cortex is lost, which results in compression fracture (**h**)

cancellous bone then supports the load, which increases both the strain and the risk of cancellous bone fracture and microfracture (Fig. 4f).

It may be difficult for scaffolding that is necessary for bone formation within the defect cavity to form. No bone is formed in the cavity, and the cavity is therefore more likely to enlarge. The strain on the cancellous bone, that supports the load at the margin of the cavity increases, bone formation becomes dominant over resorption, and the resulting bone becomes thicker (Fig. 4g). When the cavity in the cancellous bone expands, the risk of successive new microfractures in the surrounding cancellous bone increases. At the same time, the risk of fracture increases, and the beams that internally support the cortical shell that holds the vertebral bodies are lost. The cortical shell bends, which increases the likelihood of strain and microcrack deposition and results in a compression fracture (Fig. 4h).

3   Bone Remodeling and Bone Quality

3.1   Osteocytes

Osteocytes are aligned in the bone and reside in bone lacunae that are shaped like flat rugby balls ($7 \times 15 \times 23$ μm). The 3D 0.2-μm diameter tubes called canaliculi connect with adjacent osteocytes. The osteocytes form a network with blood vessels and bone marrow (Fig. 5→). Oxygen, nutrients, and calcium ions are supplied through the canaliculi. Cellular processes extending into the canaliculi are considered to be
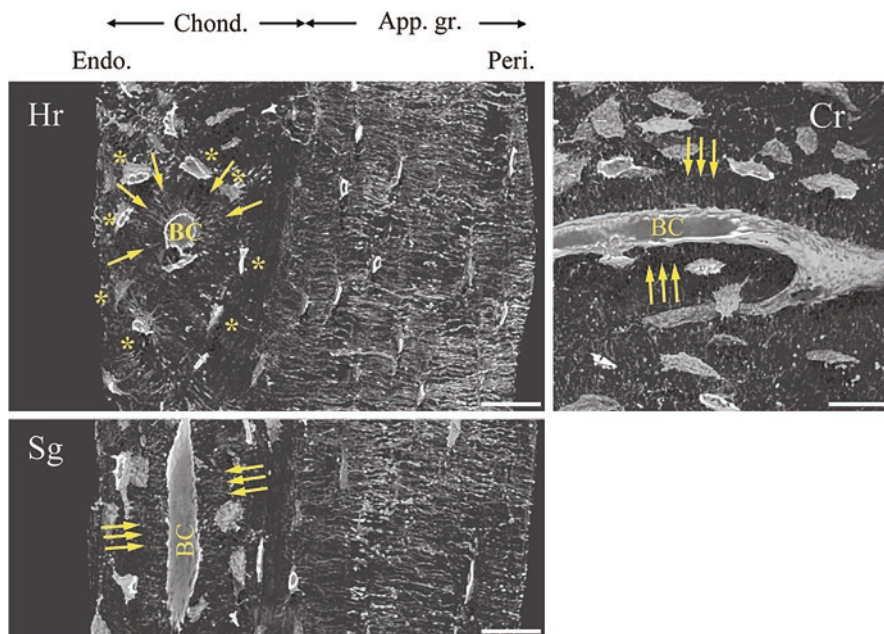
Fig. 5 The lacunar–canalicular–bone canal network. Osteocyte canaliculi connect to the bone canal (BC) throughout the endosteal cortex and are associated with bone metabolism. Note that the bone canal is surrounded by osteocyte lacunae (*) and that canaliculi ($\rightarrow$) run between osteocyte lacunae and the BC in the center. App. gr., appositional growth; Chond., endochondral ossification; Cr, coronal; Endo., endosteum; Hr, horizontal; Peri., periosteum; Sg, sagittal. Scale bar, 20 μm. (Reproduced from Nango et al. 2016 [6])

mechanosensors that respond to stress acting on bones [5]. Osteocytes are also involved in calcium resorption through mineral metabolism to maintain calcium homeostasis. And are key in the initiation of bone remodeling [6–8].

3.2   Cancellous Bone

A large amount of cancellous bone is present at sites such as the metaphysis, where an external load affects through joint. The cancellous bone of an adult consists of fine bone branches approximately 100 μm thick. It has a very large surface area per volume and is in direct contact with the bone marrow. The surface facing the bone marrow is where bone resorption predominantly occurs. The cancellous bone is thin and rod- or plate-shaped, extends in a direction that resists the load, and is constructed in a mesh to support the wall of the cortical bone.

The bone that does not support the load is resorbed and disappears, and bone that supports the load undergoes new bone formation and is remade every day to a shape adapted to stress. The cancellous bone of the femoral head extends along the principal stress line that bears the load (Fig. 6a$\rightarrow$).
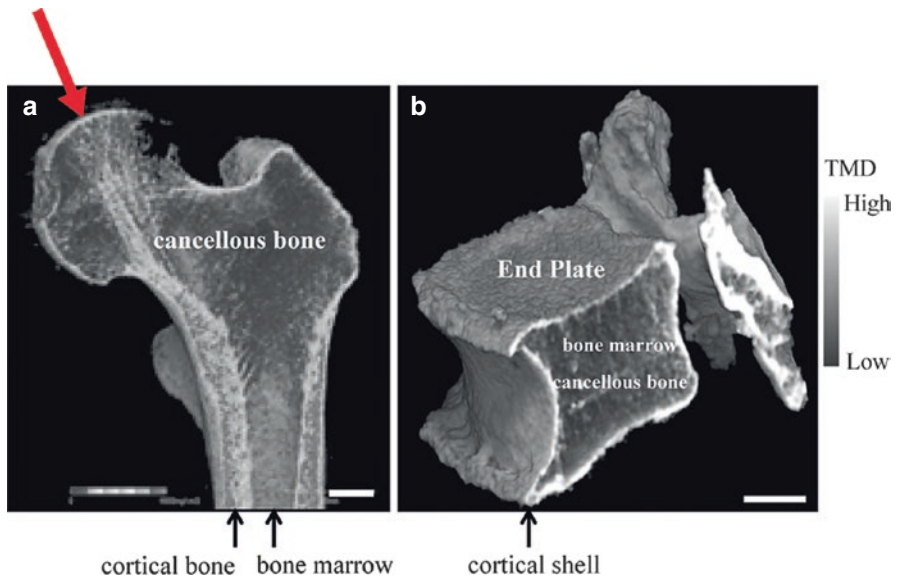
Fig. 6 Human femoral head and lumbar spine with osteoporosis. Multidetector computed tomography image. Scale bar, 10 mm. (**a**) The cancellous bone of the femoral head extends along the principal stress line that bears the load (red arrow). (**b**) A vertebral body. The cortex is thin and is called the cortical shell

3.3 Cortical Bone

The tissue that forms the outline of the bone is the cortical bone. Because the cortical bone of the vertebral body is thin, called the cortical shell (Fig. 6b). In bones that support weight, such as the femur, the central diaphysis exerts a force mainly in the longitudinal direction, and the bone consists only of cortical bone (Fig. 6a). Blood vessels run vertically and horizontally inside the cortical bone, and the bone undergoes resorption and formation.

3.4 Formation of Vertebral Bones

Vertebrae, like long bones, are formed by endochondral ossification. The vertebral end plate is cartilage that is calcified and is composed of type II collagen. The cancellous bone just below the end plate is primary cancellous bone, and the cortical bone and cancellous bone in the center of height undergo active remodeling.

3.5 Remodeling and Bone Quality

The proportion of type I collagen in the bone matrix is about 25% by weight, but the volume accounts for 70% or more. Collagen molecules extend fibers in the loading direction and form a layered structure. Needle-shaped hydroxyapatite crystals are

deposited within this structure. Hydroxyapatite crystals contribute to bone hardness, and collagen fibers contribute to the ductility of the bone. Unless the bone is resorbed, secondary calcification continues with the deposition of hydroxyapatite crystals, which makes the bone hard but quasi-brittle [9].

Bone remodeling involves the resorption of old highly mineralized bone containing microcracks and replacement with osteoid, which reduces the degree of calcification. Proper remodeling is essential for maintaining bone strength, and the distribution of calcification that depends on the remodeling frequency indirectly reflects the quality of the bone material.

The following factors are related to bone strength:

- Bone turnover
- Bone mass/bone density (bone mass refers to bone volume, and bone density refers to volume plus degree of mineralization)
- Bone material/collagen cross-linking
- Cancellous bone microstructure and cortical bone structure
- Bone mineralization distribution
- Microdamage

Of these factors, bone turnover is essential for the other factors. In bone turnover, an old bone with a high degree of calcification is replaced by a new bone with a lower degree of calcification. Collagen crosslinks are rejuvenated, and the heterogeneity of bone mineralization increases. High turnover, on the other hand, leads to transient bone loss which can become permanent if there is an imbalance of resorption and formation. Low turnover allows microcracks to accumulate, delays the formation of new bone, and increases calcified, brittle bone. To prevent fractures, optimal turnover, i.e., the balance between resorption and formation, should be maintained.

4   4DQCT

Localized mineralized bone defects expose the spine to compression fractures. The 4DQCT method detects the local porosity of calcified bone and predicts the risk of fracture. An hydroxyapatite (HA) phantom with a known degree of calcification is placed under the body for quantifying bone minerals, and MDCT imaging is performed [10].

It is possible to analyze the temporal change in bone density by converting the phantom CT value to obtain the degree of bone mineralization (Fig. 7). Bone metabolism markers directly represent the cellular activity of osteoclasts and osteoblasts. However, the specific location of the active site(s) in the body is unknown. In contrast, the 4DQCT method visualizes calcified bone, which is the result of bone resorption and formation, in three dimensions and analyzes the change over time. It is possible to visualize the occurrence and reduction of fragile sites that cannot be captured by bone metabolism markers. By observing over time the effect of medication can be visualized and can contribute to the improvement of the patient's motivation for treatment as well as the reflection on treatment efficacy.
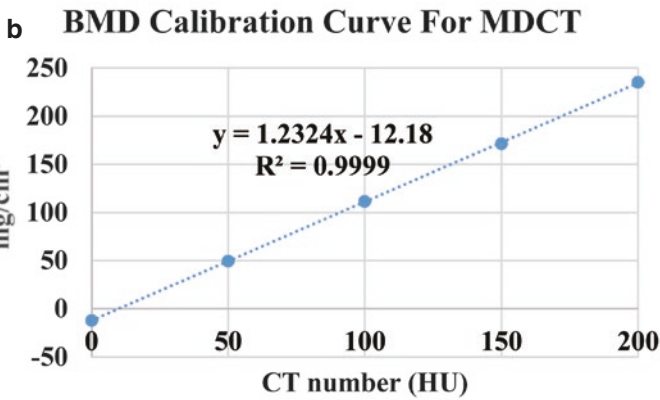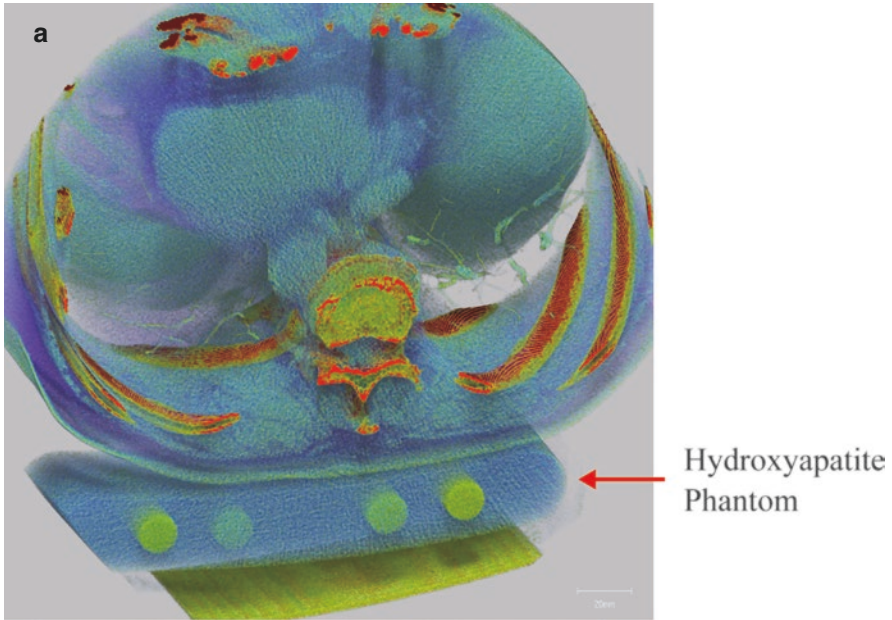
Fig. 7 4DQCT scan. The hydroxyapatite (HA) phantom is photographed at the same time and a tissue mineral density (TMD, mg/cm³) image is obtained. (**a**) HA Phantom. (**b**) TMD calibration curve

4.1 Observation of Osteoporotic Bone by MDCT

The thoracolumbar junction is known to be a site of high fracture risk. An old man walking with his waist bent may have a compression fracture. Quantification of bone fragility is important to prevent lumbar compression fractures due to osteoporosis. Conventionally, bone density measurement by DXA has been performed to measure lumbar fragility. DXA cannot detect the 3D lumbar spine structure accurately because it provides only a transmission image. On the other hand, recently, due to the development of a MDCT system, it is possible to reduce the exposure

dose and take a high-speed CT image of bone. A model with 320 rows with 0.5 mm slice thickness, a scan time of 0.5 s or less, and an exposure dose of less than twice the natural annual radiation dose has also been introduced [11].

4.2   Observation of Lumbar Cancellous Bone with MDCT

The gradation of voxels, which are points on the image captured by MDCT [11], reflects the scan resolution and the amount of bone mineral contained within the imaged point in the lumbar spine tissue. Trabeculae of the human lumbar spine have a width of 0.1 to 0.2 mm, the cortical shell width is 0.2 mm or more, and the pedicle thickness is approximately 1 mm. If the bone structure can be quantified through the use of MDCT, the bones of the whole body can be measured, and the range of application will be significantly expanded. Therefore, in the MDCT scan, the slice thickness is scanned at 0.5 mm, and the reconstruction matrix is performed at 0.2 mm, which is finer than the scan slice thickness [10]. Then, the bone measurement point becomes a 0.2-mm cube, which is close to the actual cancellous bone width, and an image that approaches the real bone can be obtained.

4.3   Measurement with MDCT and μCT Images

To examine the validity of the bone image drawn by the MDCT image scanned at 0.5 mm, the MDTC image was compared with the high-resolution μCT image. Figure 8 shows specimens of cadaveric T12 vertebral bodies imaged with μCT at a higher resolution than the width of the cancellous bone and with MDCT at a lower resolution. The MDCT images (Fig. 8a) were with 0.5 mm thickness and reconstructed at a size of 0.2 mm thickness, and the μCT images (Fig. 8b) were reconstructed with 0.05 mm voxels. The cancellous bone and cortical shell of the specimens were separated by image processing. The magnified cancellous bone image is on the right side (Fig. 8c). The color represents the degree of calcification or tissue mineral density (TMD). On μCT, the TMD is higher for the cortical shell (800 mg/cm^3) and lower for the cancellous bone (550 mg/cm^3). On MDCT, the TMD of the cortical shell is not as high as that on μCT (550 mg/cm^3), and the TMD of the cancellous bone is low (300 mg/cm^3).

In the magnified images, the cancellous bone appears thicker on MDCT than on μCT. When the MDCT image was reconstructed at a size of 0.2 mm thickness, the voxel size was 0.2 mm, but because the slice thickness of the projected image was 0.5 mm, the CT value of the bone includes part of the surrounding bone marrow. It shows that the cancellous bone shape is thick, and the TMD is low. However, when the two shapes were compared, the cortical shell contours were completely identical in terms of surface irregularities (>) and vascular cavity positions (△). The cancellous bones also matched in details such as the density difference (*), the orientation of the cancellous bone (→), and the relative difference in thickness (>>). The MDCT image therefore represents measurements of a real bone and depicts the cancellous
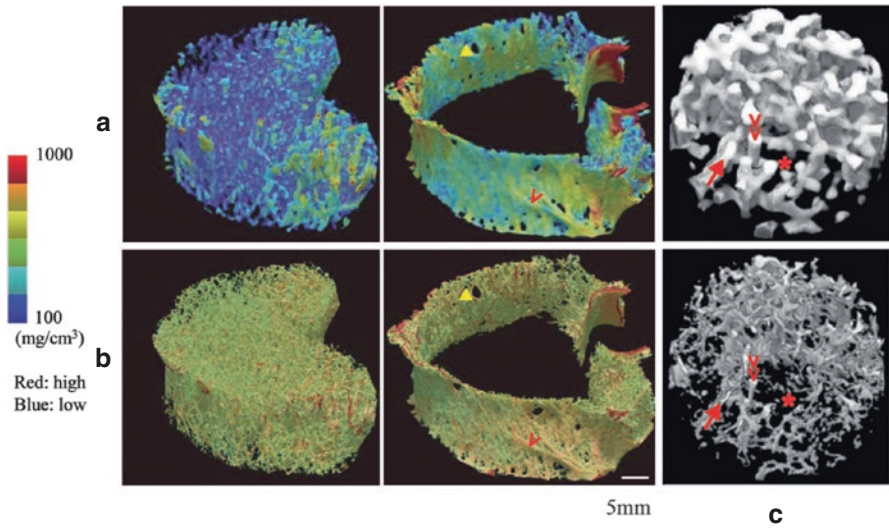
Fig. 8 Measurement with MDCT and μCT images of specimens of cadaveric thoracic vertebra T12. (**a**) The MDCT scans were with 0.5 mm slices. (**b**) The μCT scans were with 0.05 mm voxels. (**c**) Magnified cancellous bone images matching points. △: Vascular cavity. *: Defective cavity. >: Surface irregularity. >>: Thick trabecula. →: trabecula orientation

bone as a bundle of adjacent and parallel trabeculae. The cortical shells and pedicles are considered to be almost accurately represented.

4.4 Validity of 4DQCT Bone Measurement

4.4.1 Comparison of Measured Values

The validity of the bone structure measurement by means of MDCT was verified by comparison with the measurements obtained by means of μCT.

4.4.2 Sample and Method

The vertebral bodies T12, L1, L2, and L3 anatomical specimens ($N = 8$) were used. The trabecular bone and cortical bone were measured with the use of an image reconstructed at a size of 0.2 mm thickness by MDCT with a 150-mm field of view and 0.5 mm slices. For comparison as a control, we used measured values obtained from a μCT image (voxel size: 0.05 mm) with a higher resolution than that used for trabecular bone width. We converted both the MDCT and μCT images to BMD images using tissue mineral density (TMD) values as pixel values with reference the hydroxyapatite phantom. The same position was used for the analysis. In both images, the cancellous bone and cortical shells were extracted, the bone structure was measured, and a simulation of compressive loading was performed to measure bone strength.

4.4.3 Main Results

Correlation of Degree of Calcification TMD

The TMD at the same point on the MDCT image and the μCT image was obtained, and the correlation was investigated [9]. The degrees in cancellous bone were correlated significantly between the two imaging modes ($R^2 = 0.74$, $p < 0.01$; Fig. 9). The same results were obtained for the cortical shell [12].

Bone Structure Measurements

The data from the MDCT and μCT images for many measurements—such as the bone volume fraction (BV/TV), the star volume of bone marrow space (V* m.space),
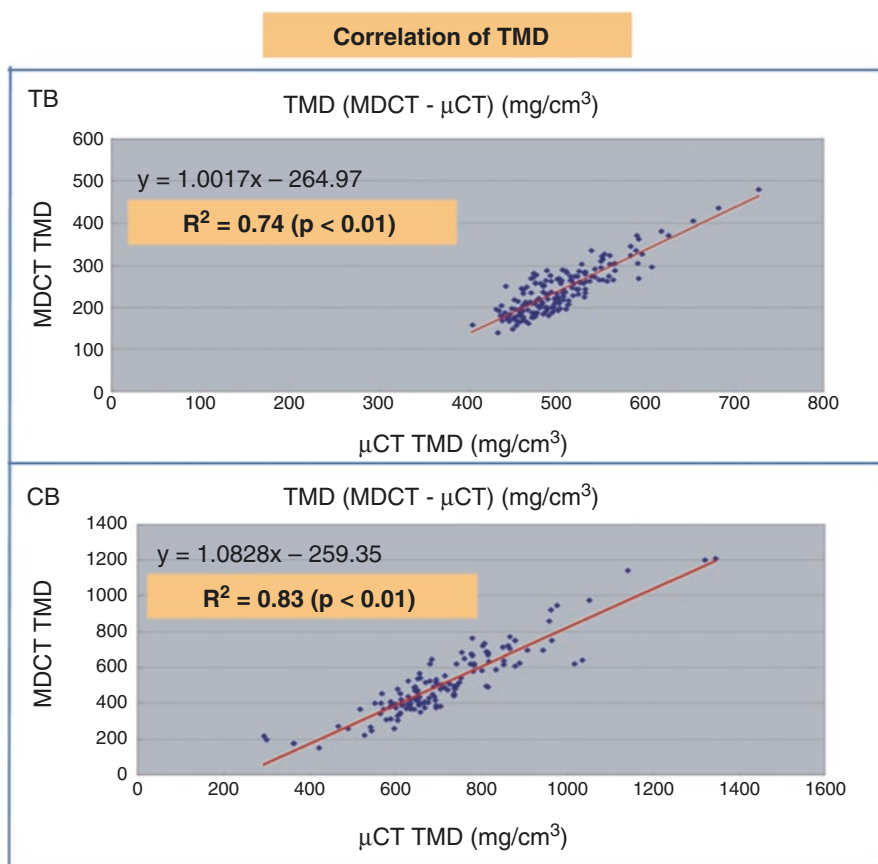
Fig. 9 Tissue mineral density (TMD) correlation. TMDs at the same point on multidetector computed tomography (MDCT) and computed tomography with μCT were correlated. The degree of cancellous bone calcification using MDCT images correlated with that of μCT images ($R^2 = 0.74$, $p < 0.01$) (TB; upper). The same was true for cortical bone (CB; lower)

trabecular star volume (V* tr), trabecular thickness (Tb.Th), trabecular number (Tb.N), mean intercept length (MIL), and degree of anisotropy (DA)—were highly correlated, BV/TV ($R^2 = 0.76$, $p < 0.009$). Node-strut measurements showed a low correlation N.ND/TV ($R^2 = 0.22$, $p < 0.01$). We, therefore, concluded that the bone structure measurements obtained with MDCT image reflected the true value of the bone, although the image resolution of MDCT was lower than the thickness of trabecular bone.

Stress Simulation

The results of the fracture load simulation on MDCT images were correlated significantly with those on µCT images ($R^2 = 0.7$, $p < 0.09$; Fig. 10) [12].
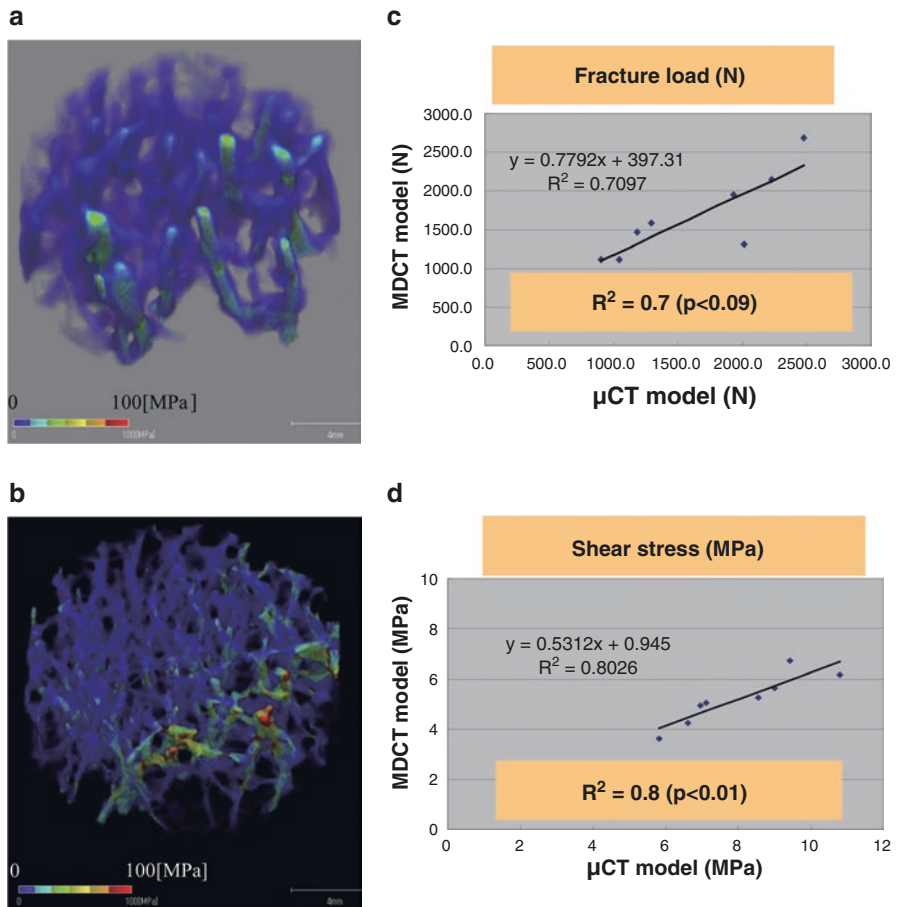
Fig. 10 Stress simulation. Results of fracture load simulation on multidetector computed tomography (MDCT) image were correlated with simulation results on computed tomography with the µCT image ($R^2 = 0.7$, $p < 0.09$). (**a**) Shear stress of MDCT model. (**b**) Shear stress of µCT model. (**c**) Fracture load. (**d**) Shear stress

5   4DQCT Measurement

5.1   Degree of Mineralization

In 4DQCT, an X-ray image is created with the use of the linear absorption coefficient (attenuation rate per unit path length) of the bone to X-ray. X-ray images are displayed with bright hard dots and dark soft dots. This appearance is used to measure the degree of bone mineralization and bone density.

The degree of mineralization is described as TMD according to the guidelines of the American Society for Bone and Mineral Research [13], and the mineral density in tissues, including bone marrow, is expressed as volumetric BMD (vBMD), which is a value obtained by expanding the bone density (mg/cm^2) measured with DXA into three dimensions (mg/cm^3). The bone density of the DXA image is expressed as areal BMD (aBMD) because it normalizes the measurement only by area.

TMD is the amount of mineral in marrow-free bone. An HA Phantom with a known TMD value is scanned with the bone, and the TMD value (mg/cm^3) of the bone is calculated. A TMD threshold L is used to identify bone, and then the number N of points (voxels) that show bone tissue with a value of L or more is counted, and the bone volume is calculated as $BV = N \times$ one voxel volume. To calculate the total amount of bone mineral content (BMC, in milligrams), the average TMD value of bone is multiplied by the bone volume:

$$\mathrm{BMC}\left(\mathrm{mg}\right) = \mathrm{TMD\ mean\ value}\left(\mathrm{mg/cm^3}\right) \times \mathrm{BV}\left(\mathrm{cm^3}\right).$$

Thus, the bone TMD is BMC/BV.

5.1.1   Volumetric Bone Mineral Density (vBMD; mg/cm³)

Mineral density in the total volume TV (in cc^3), which is the bone marrow tissue that includes bone, is calculated as follows:

$$\mathrm{vBMD} = \mathrm{BMC/TV}\left(\mathrm{mg/cm^3}\right) = \mathrm{TMD} \times \left(\mathrm{BV/TV}\right).$$

Both the reduction of bone volume and mineralization are taken into consideration, and the result is an accurate indicator of osteoporosis.

The bone depicted in Fig. 1c was fragile as a result of extreme osteoporosis. However, the cancellous bone TMD was large. Because TMD indicates the hardness of the remaining bone, the volume ratio of the bone to the TV is not included in the calculation of TMD. TMD does not represent mechanical strength. On the other hand, the calculation of vBMD includes both TV and bone mass, and large vBMD is correlated to high mechanical strength [14].

The vBMD (mg/cm^3) measured with MDCT images was correlated with areal BMD (mg/cm^2) measured with DXA ($R^2 = 0.74$, $p < 0.01$) [15].

Figure 6 shows gray value images of the degree of calcification in a femur and a vertebral body. The femoral head obviously has a low degree of calcification, the femoral neck shows worsening porosity, and the diaphysis has a high degree of calcification.

### 5.1.2   Measurement of Treatment Effect by Bone Mineral Density

The vBMD is a 3D measurement, and the value does not depend on the direction of CT imaging. In addition, the cancellous bone and cortical shell can be depicted separately, and site-specific changes in bone density, such as a significant increase or decrease in cancellous bone mineralization, can be measured.

Because a voxel on the MDCT image is larger than a trabecular width, the TMD value of the cancellous bone voxel includes the value of the bone marrow space, in addition to the cancellous bone. The value is smaller than the mineral density of true cancellous bone. However, it is possible to express changes such as improvement resulting from medication and to make comparisons between cases, between bone sites, and between rates of bone resorption and formation, and these values express changes in the lumbar spine in osteoporosis [10].

5.2   Measurement of Treatment Effect by Bone Morphometry

MDCT images can quantitatively show changes in the bones of a patient during treatment. Figure 11 depicts a case of drug intervention with the bone formation promoter teriparatide for 1.5 years. The star volume value is displayed in pseudo-color for each point, this is called the star volume map. The images on the left were obtained before treatment, and those on the right were obtained after treatment. The upper image is V* tr, and the lower image is V* m.space. Dosing increased V* tr red (>) and decreased V* m.space red (→). The 3D star volume shows that the cancellous bone thickness increases, the defective cavity shrinks, and bone formation in the direction of the supporting load is accelerated. Administration of teriparatide improved V* tr by 40%. V* m.space improved by 9% (Fig. 11).

Fig. 11 Treatment effect measurement by bone star volume: The star volume value is displayed in pseudo-color for each point, this is called the star volume map. The star volume map can visualize the improvement of local structural changes after treatment. >: Increased V* tr. →: Reduced V* m. space
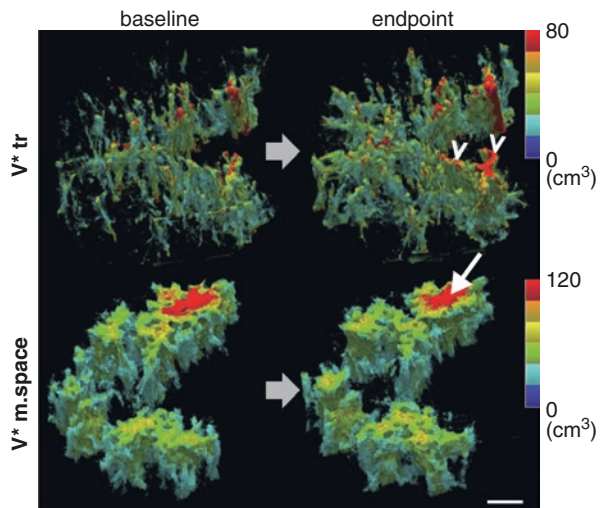
Inoue et al. showed improvements of V* m.space and fracture load using bisphosphonates for glucocorticoid osteoporosis and using MDCT images to measure the therapeutic effect [16].

6 Bone Morphometry Indexes

3D bone morphometry is used to measure the fine structure of trabecular and cortical bone, which are components of bone quality.

Bone morphometry is divided into cancellous bone morphometry of the bone metaphysis near the joint and cortical bone measurement of the diaphysis without cancellous bone in the middle of the long bone diaphysis.

6.1 3D Cancellous Bone Morphometric Index

6.1.1 Trimming Measurement Area

The number of metaphyseal trabeculae in the long bones is significantly reduced with the distance from the growth plate. When comparing the amount and quality of bone between samples, it is important to compare bones at the same site to reduce the comparison error. Therefore, the same part is compared in the same direction. In the example (Fig. 12), the anterior side of the tibia of the mouse faced upward, and the diaphysis was set up vertically.

Based on the bottom edge of the growth plate, a length of 0.2 mm was offset to avoid the primary cancellous bone, and the distal 2 mm was set as the measurement range (Fig. 12).

6.1.2 Trabecular Bone Morphometry

Below, a decrease in the index due to changes in bone mass is indicated by ($-$) and an increase is indicated by ($+$).

The measurements assessed in trabecular bone morphometry are listed as follows:

①TV (mm^3) Total Volume: Cancellous bone measurement area volume (bone marrow + bone volume). The cancellous bone to be measured is defined as the bone that is included in the bone marrow tissue. The index of the bone whose value changes depending on the size of the measurement site is divided by TV and normalized to be used for comparison between samples.

②BV (mm^3) Bone Volume: Cancellous bone volume is calculated by counting the number of voxels that make up the cancellous bone. Since the value depends on the ROI range, it is normalized by TV and used for sample comparison.

③BS (mm^2) Bone Surface: Cancellous bone surface area. On imaging, a triangular patch is laid out on the bone surface, the bone surface area is the sum of the triangular surface areas. And another measurement method of BV is the volume inside the patch.
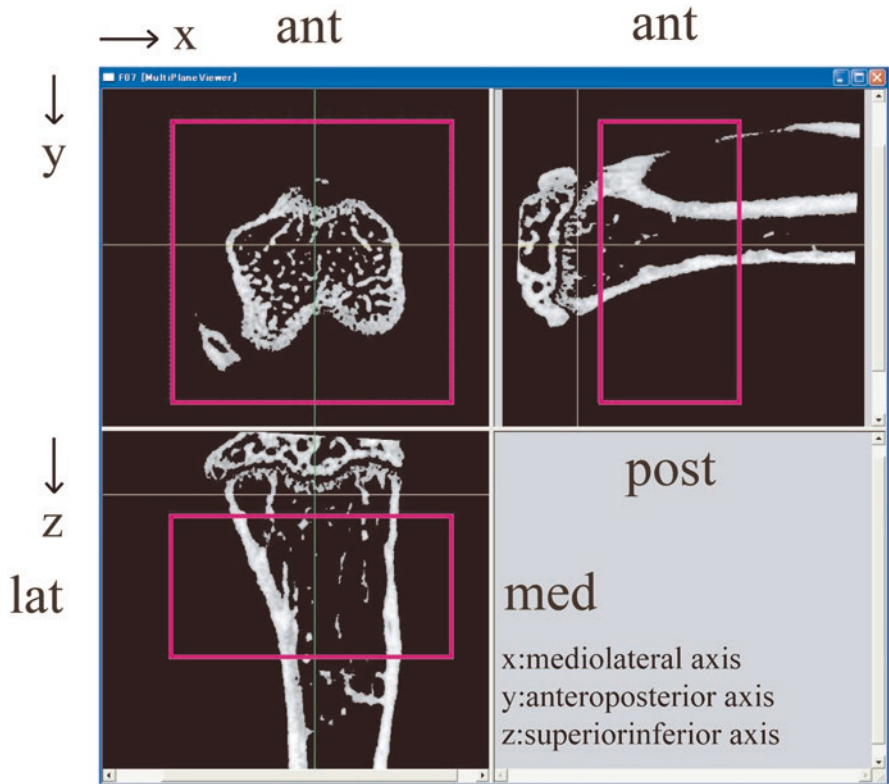
Fig. 12 Measurement area definition. Based on the bottom edge of the growth plate, a length of 0.2 mm was offset to avoid the primary cancellous bone, and the distal 2 mm was set as the measurement range

④BV/TV (%) Bone Volume Fraction: Most often used for comparisons between samples.

⑤BS/TV (mm²/mm³) Bone Surface-to-Total Volume Ratio: Used for comparison between samples of bone resorption surface.

⑥BS/BV (mm²/mm³) Bone Surface-to-Bone Volume Ratio: Comparison of erosion on the bone surface. The increase in the index is a result of an increase in bone resorption surface.

⑦Tb.Th, Tb.Th.SD (μm) Trabecular Thickness, Standard deviation: Cancellous bone width and standard deviation (Fig. 13a). Tb.Th is defined by the direct measurement method as the average of the diameters of the maximal spheres fitting inside the structure [17]. The spatial distribution of Tb.Th demonstrates that when the cancellous bone is thinned and contains holes, the number of rod-shaped trabeculae increases (Fig. 2). Since Tb.Th does not depend on the measurement ROI range, normalization is unnecessary.
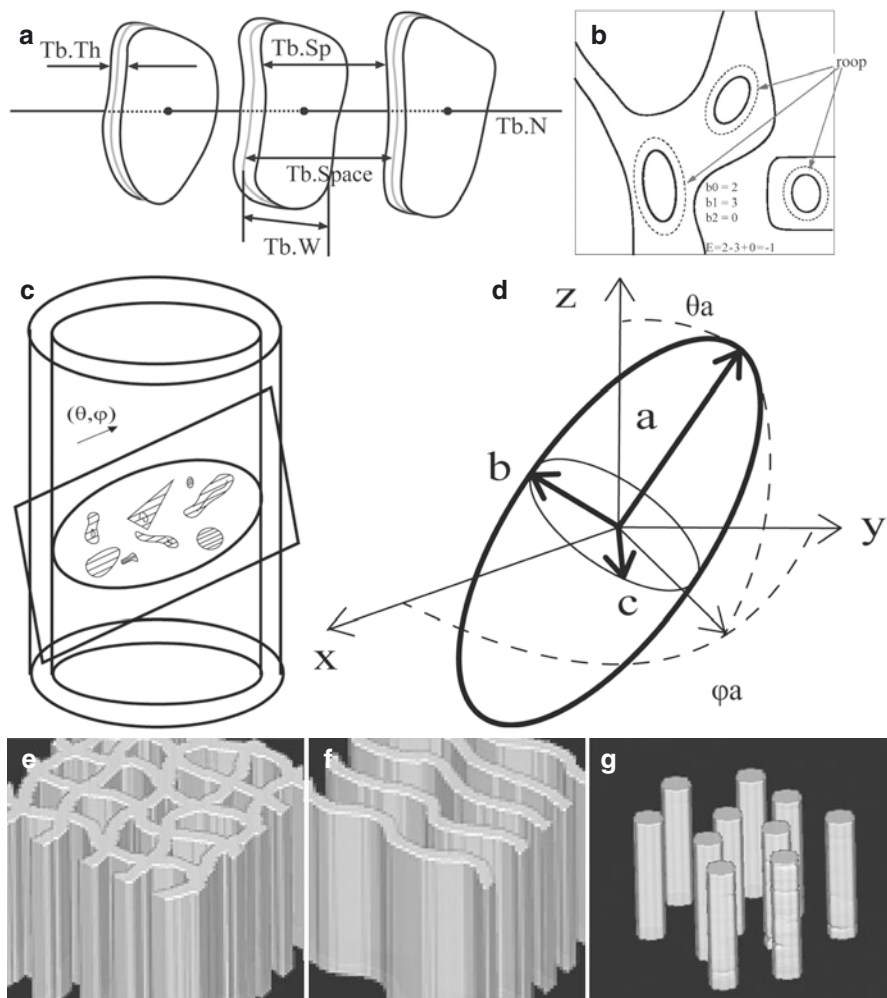
Fig. 13 Trabecular bone morphometry. (**a**) Trabecular bone dimension definition. Tb.N: Trabecular number, Tb.Sp: Trabecular separation, Tb.Space: Trabecular space, Tb.Th: Trabecular thickness, Tb.W: Trabecular width. (**b**) In rod-shaped bone, the loop formed by the connecting cancellous bone expresses connectivity density (Conn.D). (**c**) MIL (θ, φ): average value of bone crossing length in the direction of (θ, φ). (**d**) Ellipsoid approximating MIL (θ, φ), same moment of inertia: composed of major axis radius a, intermediate axis radius b, minor axis radius c, and major axis direction (θa, φa). The degree of anisotropy is a/c. (**e**) Honeycomb-shaped bone. TBPf <0; SMI $\fallingdotseq$ 0. The bone marrow is divided into this formation by plate-shaped cancellous bone. (**f**) The cancellous bone forms a plate shape. TBPf $\fallingdotseq$ 0; SMI $\fallingdotseq$ 0; SMI: Structure model index, TBPf: Trabecular bone pattern factor formation by plate-shaped cancellous bone. (**g**) The cancellous bone forms a rod shape. TBPf >0; SMI $\fallingdotseq$ 3.0. (**h**) Before perforation. (**i**) After perforation. V* m.space: Star volume of the bone marrow space (V* m.space [red]). V* tr: Linear spread volume in the trabecular bone is shown (V* tr, trabecular star volume [black]). With regard to linear spreading volume in cancellous bone, when a plate-shaped cancellous bone is perforated, the star volume changes significantly more than does perforation volume, and the sensitivity to perforation is high. (**j**) Node-strut: cancellous bone network and cortical bone junction are shown. Nd: Node, Tm: Terminus
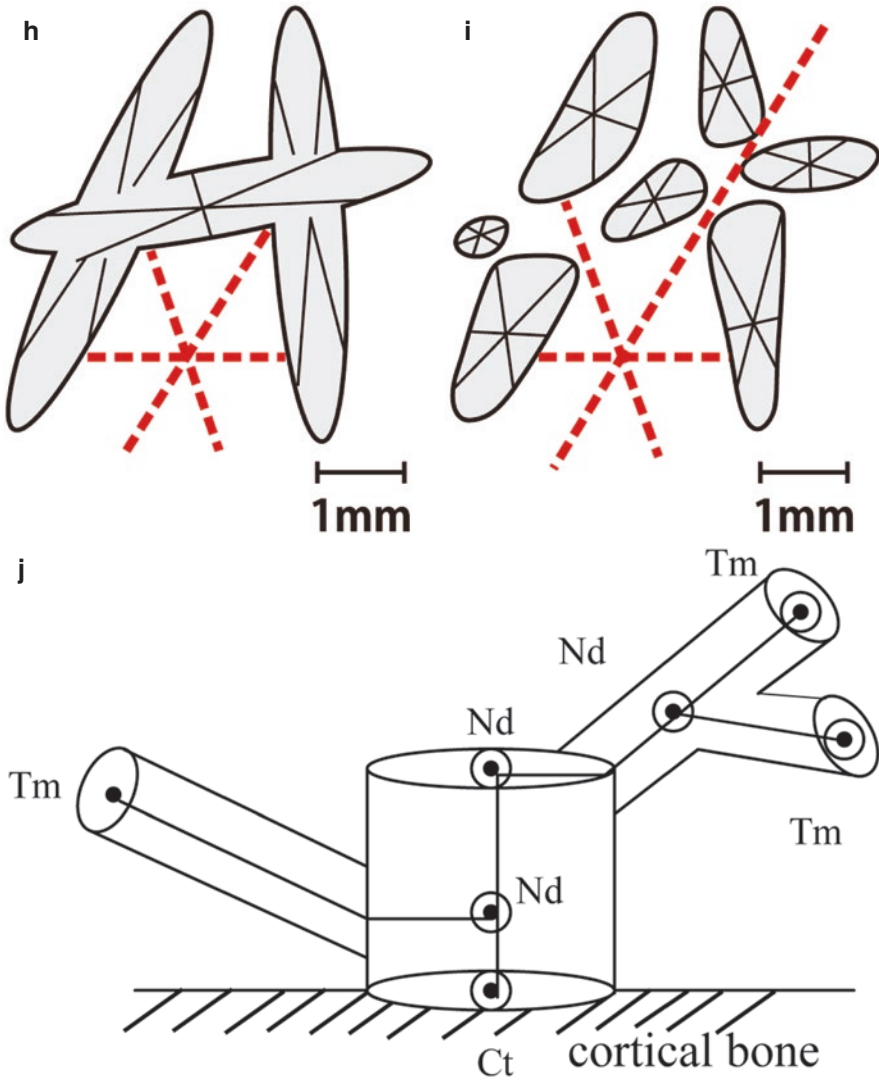
Fig. 9.13 (continued)

⑧Tb.Sp, Tb.Sp.SD (μm) Trabecular Separation, SD: Distance between the cancellous bone surfaces and the standard deviation. With the progress of osteoporosis, these indexes increase. They are calculated by a direct measurement method of the bone marrow space.

⑨Tb.N (1/mm) Trabecular number: Number of trabeculae.

The number of bones passing per unit length is counted using a measurement line on a cross section orthogonal to the bone extension direction. In the plate model calculation, it is calculated as follows:

$$\text{Tb.N} = \left(\text{BV} / \text{TV}\right) / \left(\text{Tb} \cdot \text{Th}\right).$$

⑩Conn.D ($1/\text{mm}^3$) Connectivity Density is an index of bone connectivity (Fig. 13b). In the rod-shaped bone, the connecting trabeculae form a loop. In the case where the cancellous bone in the bone marrow has $b0$ connected components, $b1$ loops, and $b2$ cavities, the Euler number χ of the bone structure can be obtained with the following formula:

$$x = b0 - b1 + b2.$$
$$\text{Conn.D} = \left(1 - x\right) / \text{TV} \cong \left[1 - \left(1 - b1 + 0\right)\right] / \text{TV} = b1 / \text{TV},$$

where $b0 = 1$ and $b2 = 0$. $b0$ and $b2$ may have an error that counts random noise generated in CT imaging, $b1$ is unlikely. Therefore, the connected component $b0$ is approximated to 1, and the number of cavities $b2$ is approximated to 0. In the case of the rod-shaped bone, cancellous bone connectivity is high when there are many cancellous bone loops. The value decreases with increased porosity. However, this is not the case with plate-shaped bones. Incidentally, χ is a mathematical invariant whose value does not change due to the expansion or contraction of the shape.

⑪DA Degree of Anisotropy: Defined according to the MIL ellipsoid, for which MIL represents transverse bone length. The length of a straight line passing through an arbitrary point in the trabecular bone is obtained, and the average is obtained for each direction (Fig. 13c).

MIL(θ, φ): Average bone crossing length in the (θ, φ) direction, where the angle θ is formed by the crossing line with the z-axis and the angle φ is formed with the x-axis. It is approximated by an ellipsoid whose moment of inertia matches with MIL. The MIL ellipsoid is composed of a major axis with radius a, an intermediate axis of radius b, a minor axis radius c, and a major axis direction (θa, φa) (Fig. 13d):

$$\text{DA} = a / c.$$

A DA of 1.0 has no anisotropy, and the vertebral body increases anisotropy when osteoporosis worsens.

⑫Plate–rod shape index: In a young person, the cancellous bone of the vertebral body has a honeycomb structure with many concave structures. As osteoporosis progresses, the honeycomb-like structure changes to a plate-shaped structure and eventually becomes rod shaped. The structure model index (SMI) and trabecular bone pattern factor (TBPf) index represent the stages of this progress (Fig. 13e–g). The SMI is 0 for an ideal plate shape, 3 for a rod shape, and 4 for a sphere [18]. For the TBPf, the amount of change in the surface area with regard to the change in the volume expansion near the surface of the trabecular bone in 3D space is used as an index. When the volume increases, the change in surface area (ΔS) becomes negative in the honeycomb bone, becomes 0 in the plate bone, and becomes positive in the rod bone:

TBPf = ΔBS/ΔBV (mm^2/mm^3), where ΔBS is the change in surface area and ΔBV is the change in volume.

⑬3D star volume: 2D star volume [19] is expanded to 3D.

(a) V* m.space (mm^3) Marrow space star volume: Bone marrow star volume.

The volume of the bone marrow cavity that can be seen from the point in the bone marrow cavity in all directions without being obstructed by the trabecular bone. It is defined by the following formula (Fig. 13h, i [dotted line part]):

$$V * m \cdot space = \pi / 3 \times L_0^{\,3},$$

where L_0: At a point in the medullary cavity, the length of a straight line passing through the point across the medullary cavity is determined and averaged in all directions. Values are then averaged for points in the bone marrow.

A large value is obtained when the cancellous bone is locally missing.

It is an index that best reflects the deterioration of bone.

(b) V* tr (mm^3) Trabecular star volume: The average of the volume in the linear range from the point in the trabecular bone to the end of the trabecular bone. It is defined by the following formula (Fig. 13h, i [solid line part]):

$$V * tr = \pi / 3 \times \sum L_1^{\,4} / \sum L_1,$$

L_1: Obtain the straight line distance from one end to the other through the point in the cancellous bone, and take the average in all directions. The values are then averaged for points in the bone. The more holes there are, the smaller the value. It expresses the degree to which cancellous bones are connected in a straight manner. When the cancellous bone in Fig. 13 (h) is perforated and becomes (i), V* m.space increases remarkably and V* tr decreases remarkably exceed the absorption volume. 3D star volume has a high sensitivity to perforation.

In the presence of cancellous bone random, since the 3D star volume does not depend on the ROI range, there is no need for normalization and it is the absolute value of the morphology.

⑭Node-strut: Measurement of the skeletal line network of cancellous bone branches. The state of cancellous bone branch is expressed by the branch point (N.Nd/TV), cortical bone point (N.Ct/TV), and branch length (TSL/TV). These indices decrease (−) when the cancellous bone branch decreases in rod-shaped bone (Fig. 13j).

6.2   Cortical Bone Morphometry

A cross section orthogonal to the growth direction is measured mainly in the diaphyseal cortical bone (Fig. 14a, b). As the protrusion of the convex portion of the front edge of the tibia is an error factor, avoid it, and measure a constant part of the triangular cross section. In the measurement of porosity, an error of counting bone marrow cavity is likely to occur in the tens of microns on the endosteal side, so it is excluded from the measurement range. Avoid a few tens of microns on the periosteal side as well. For simplicity, the metaphyseal cortical bone is also measured. To

reduce the error, several cross sections in the height direction are measured and averaged.

①Tt.Ar (mm^2) Total cross-sectional area: Total cross-sectional area of the cortical bone, including the bone marrow.

②Ct.Ar (mm^2) Cortical bone area: Cortical bone cross-sectional area.

③Ct.V (mm^3) Cortical volume: Ct.Ar × number of cross sections measured × cross section thickness.

④Ma.Ar (mm^2) Medullary area: Cross-sectional area of the bone marrow.

⑤Ct.Ar/Tt.Ar (%) Cortical area fraction: Ratio of the cortical bone to the total cross-sectional area.

⑥Ct.Th (mm) Average cortical thickness: Cortical bone thickness calculated by direct measurement [17].

⑦Ps.Pm (mm) Periosteal perimeter: The perimeter of the outer membrane.

⑧Ec.Pm (mm) Endocortical perimeter.

The perimeter of the inner membrane.

Geometric moment of inertia.

The areal moment of inertia is expressed as $I = \Sigma r^2 \mathrm{d}s$, where r is the distance to the measurement axis, and ds is calculated according to the pixel cross-sectional area (Fig. 14c).

⑨I_{ap} (mm^4) Moment of inertia about the anteroposterior axis: Moment of inertia related to bending strength in the anterior–posterior direction. It is the second moment of r_y that emerges from the cortical bone in the anterior–posterior (y) direction to normal axis x (Fig. 14c).

⑩I_{ml} (mm^4) Moment of inertia about the mediolateral axis: The second moment of r_x that goes inward and outward direction distance to normal axis y, from the cortical bone. It is related to the bending strength when a load is applied from the lateral side, with the medial side as the fulcrum.

⑪I_{max}, I_{min} (mm^4) Maximum, Minimum moment of Inertia: Maximum and minimum values of the moment of inertia when changing the angle φ of the measuring axis (Fig. 14c).

⑫J (mm^4) Polar moment of inertia: Second moment of r_p from the cortical bone to the center of gravity of the cross section (Fig. 14c).

It is related to torsional strength.

⑬Po.V (mm^3) Total pore volume.

⑭Po.N (n) Pore number: Number of porosities in the cortical measurement section. The small pore size is comparative to the pixel size of the image. So the number of porosities is prone to error.

⑮Ct.Po (Volume%) Cortical porosity ≡ Po.V/Ct.V (%): Volume ratio of porosity, measured as volume percentage. Volume is little influenced by random noise and can be used for sample comparison.

⑯Avg Po.V, SD (mm^3) Average Pore Volume (≡ Po.V/Po.N): Average volume of the porosity and standard deviation.

⑰ Po.Dn (1/mm^3) Pore density (≡ Po.N/Ct.V): Porosity number density. The number of pores in the cortical bone is not considered accurate because the detection of minute pores depends on the CT image resolution. Also, vulnerable to random noise.
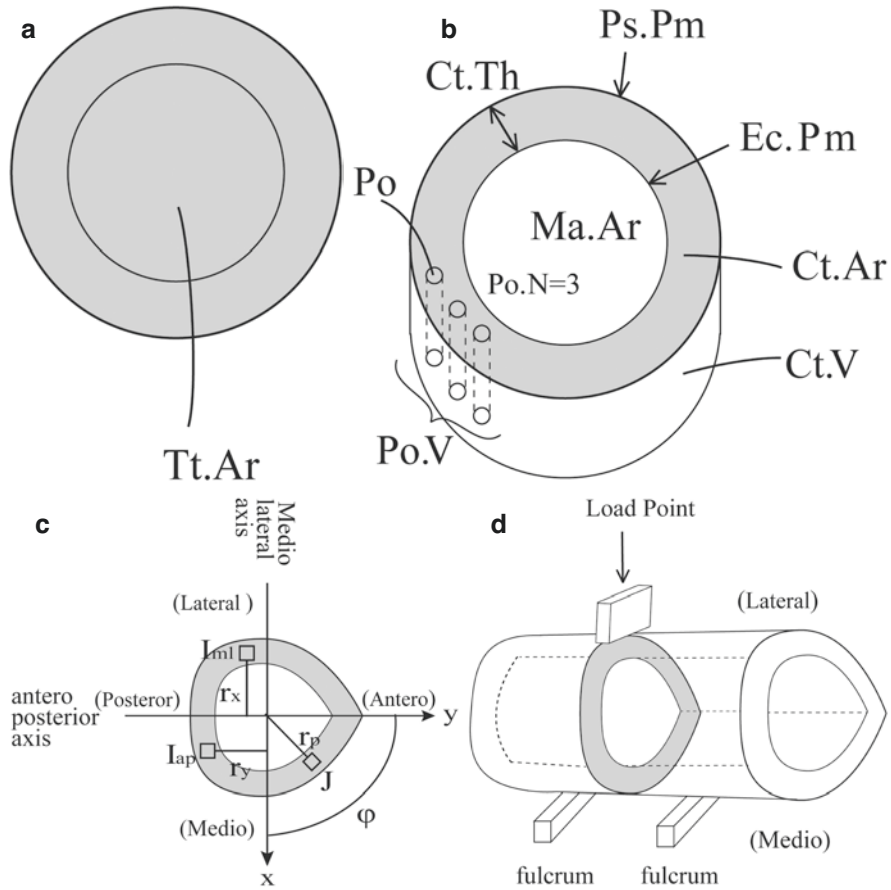
Fig. 14 Cortical bone morphometry. (**a**) Cortical bone cross-sectional. Tt.Ar: Total cross-sectional area. (**b**) Definition of cortical bone morphology measurement items. Ct.Ar: Cortical bone area, Ct.Th: Average cortical thickness, Ct.V: Cortical volume, Ec.Pm: Endocortical perimeter, Ma.Ar: Marrow area, Po: Pore, Po.N: Pore number, Po.V: Total pore volume. (**c**) Definition of cortical bone moment of inertia. X: Represents the mediolateral axis. Y: Represents the anterior–posterior axis. r_x: distance to y axis. r_y: distance to x axis. r_p: distance to center. □: cross-sectional area. φ: angle of the measuring axis. (**d**) Three-point bending test in the mediolateral direction

6.3   Changes in 3D Index Due to Spongiosa Osteoporosis

The 3D bone morphometric index expresses quantity, shape, connectivity, and bone mineralization. Osteoporosis significantly alters bone structure. The bone morphology index can be used to determine the risk of vertebral body fracture. The changes brought about by the trabecularization of the cancellous bone in the 3D morphometric index are summarized in Fig. 15 and Table 1.
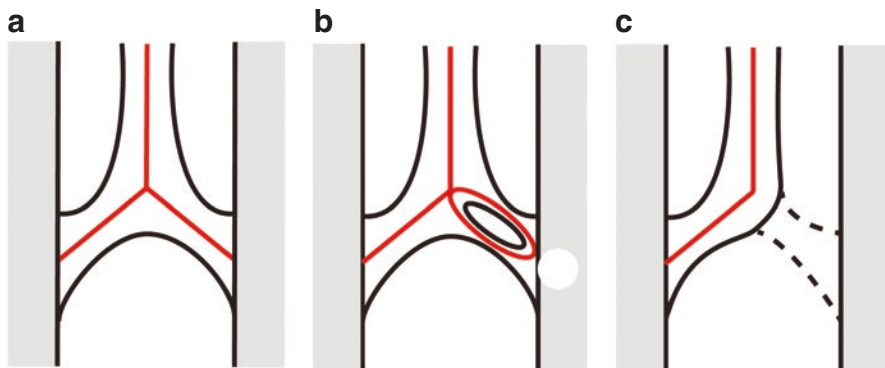
Fig. 15 Change in 3D cancellous bone parameter index as a result of cancellous osteoporosis. Red lines indicate skeleton. (**a**) Schema of plate-shaped cancellous bone. (**b**) Schema of perforation occurrence, in which *b1* is +1, node-strut (NdNd) is +1, the bone volume fraction (BV/TV) and trabecular thickness (Tb.Th) remain unchanged, and star volume of bone marrow space (V* m.space) increases. (**c**) When the cancellous bone branch is missing, *b1* is −1, NdNd is −1, BV/TV is decreased, Tb.Th is unchanged, and V* m.space is increased. V* m.space increases both when perforation occurs and when cancellous bone is lost and is an sensitive indicator of osteoporosis

BV/TV and Tb.Th decrease gradually with age but decreases sharply in patients with osteoporosis. However, these indexes are less sensitive to plate bone perforation and loss of rod-shaped bone.

Conn.D and node-strut (N.Nd/TV) increase once healthy plate-shaped bone is perforated and becomes rod-shaped, and then, they decrease in accordance with the porosity. Until the bone becomes rod-shaped, these indexes do not reflect porosity.

TBPf and SMI express the transition of the bone from honeycomb-like to plate shaped and from plate shaped to rod shaped. However, these indexes are less sensitive to thinning of the plate-shaped bone, the process of perforation of the plate-shaped bone before osteoporosis, and cancellous bone loss after the deterioration of porosity.

On the other hand, 3D star volume V* m.space reflects any stage of gradual bone loss due to aging, change from the honeycomb shape to plate shape, thinning of plate bone, perforation, rod ossification, and rod bone loss. And, it is more sensitive to bone loss than the decrease in bone mass (BV/TV) and increases as bone porosity increases. In the presence of cancellous bone random, the value does not change depending on the measurement ROI selection or size, so it is an absolute value that represents a shape that does not require normalization.

6.4   Finite Element Analysis

The bone data can be extracted from the CT image, and a finite element analysis model with one voxel as a hexahedron can be created. A finite element analysis

Table 1 Changes in 3D index due to spongiosa osteoporosis

(a) Trabecular bone is less affected by plate bone perforation and rod bone defects.
(b) The index increases when the shape of the bone changes from a plate into a rod, and it is reduced when rod-shaped bone is lost. It does not reflect porosity until the bone becomes rod-shaped.
(c) The change from plate bone to rod bone does not reflect the effects of rod bone defects, since the bone surface does not change.
(d) The value always rises with the deterioration of porosity. 3D star volume of bone marrow space (V* m.space) is a simple, accurate index of osteoporosis.
3D star volume V* m.space is simple and excellent as an index of osteoporosis.

model of cancellous bone can be easily created with CT images. Young's modulus of the model is given using the bone TMD values [20].

In finite element analysis, it is possible to perform a load test simulation in a specific direction with consideration of muscle function, a compression test, a three- or four-point bending test, a torsion test, or a load test of a bone with an implant, which is difficult in an actual destructive test. Given a fixed point, a load point, a load direction, and a load magnitude, the static solution is obtained. Displacement, principal stress, shear stress, principal strain, and shear strain are calculated for each element, and the elastic constant of the bone structure is obtained. The fracture load can be obtained by defining the fracture condition by strain or stress.

6.4.1 Stress Simulation Using MDCT Images

MDCT imaging was performed using a cadaveric specimen sample ($N = 9$), and bone morphology measurement and FEA compression simulation were performed. The point where the shear stress exceeded 60 MPa was defined as a fracture.
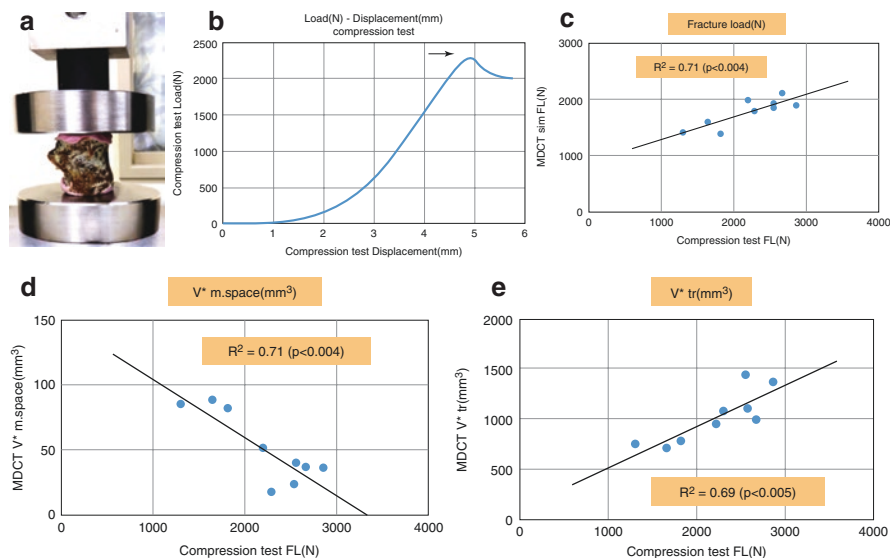
Fig. 16 Correlation between vertebral body of cadaveric specimen compression test and multidetector computed tomography (MDCT) image simulation (sim). Fracture load (FL) calculated with quantitative computed tomography stress simulation was correlated with the results of a compression test (**a, b, c**). The 3D star volume was correlated with the fracture load in the compression test (**c, d**). V* m.space: Star volume of bone marrow space; V* tr: Trabecular star volume. FL: Fracture Load. (**a**) Cadaveric specimen Compression test. (**b**) Maximum load (→). (**c**) Simulation, compression test correlation

In addition, a mechanical compression test was carried out using a compression tester EZGraph (Shimadzu, Kyoto, Japan) to determine the maximum load (Fig. 16a).

The maximum load was defined as the breaking load (FL) (Fig. 16b→).

The fracture load obtained by stress simulation using MDCT images was highly and significantly correlated with the fracture load of the compression test (Fig. 16c).

The results of star volume measurement of all bones including the cortex were correlated with the compression fracture load and $R^2 = 0.71$ ($p < 0.004$) for V* m.space and $R^2 = 0.69$ ($p < 0.005$) for V* tr (Fig. 16d, e).

6.4.2 Three-Point Bending Test Simulation and Fracture Test Comparison

Figure 17a illustrates a three-point bending test with a rat femur, and Fig. 17b illustrates a simulation model obtained with μCT. Figure 17c depicts the simulation results of a three-point bending test and shows the correlation between the fracture load obtained from the simulation under a 68-MPa load and the maximum load at fracture obtained in the fracture test ($N = 12$). The results of both tests showed significant correlations of $R^2 = 0.76$ ($p < 0.01$).
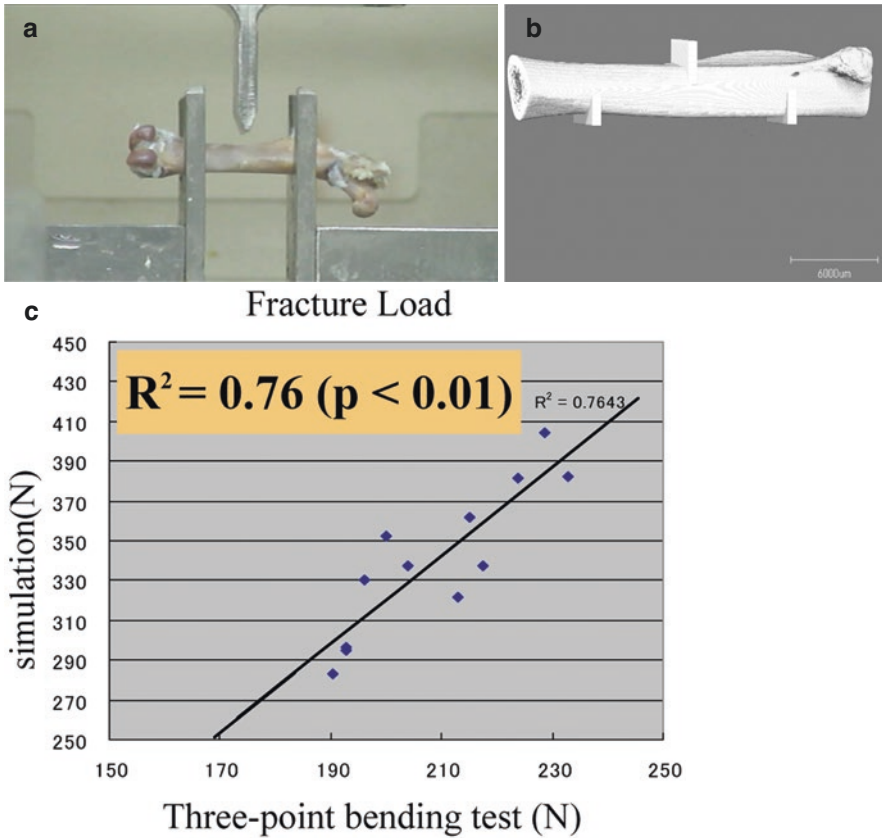
Fig. 17 Finite element analysis. (**a**) Three-point bending test with a rat femur. (**b**) A model for simulation. (**c**) A graph of the results. The fracture load obtained by stress simulation is correlated with the result of the three-point bending test ($R^2 = 0.76$, $p < 0.01$)

7   Age-related Mouse Bone Growth [21]

Figure 18 and Table 2 show growth with age of wild-type mice2,4,6,8,12,14, and 28 weeks old ($N = 3$/age). A 0.2-mm offset was taken from the growth plate to avoid primary cancellous bone, and 1.5 mm height was measured.

Up to 8 W, bone shape (Tt.Ar), cancellous bone volume (BV), cortical bone area (Ct.Ar), and bone mineral content tend to increase with age. At the ages of 8 to 12 weeks, the outer shape of the bone (Tt.Ar) does not change further, the pores within the cortex are filled, the cancellous bone becomes thicker (Tb.Th), and bone quality changes. TMD continues to increase up to the age of 28 weeks.
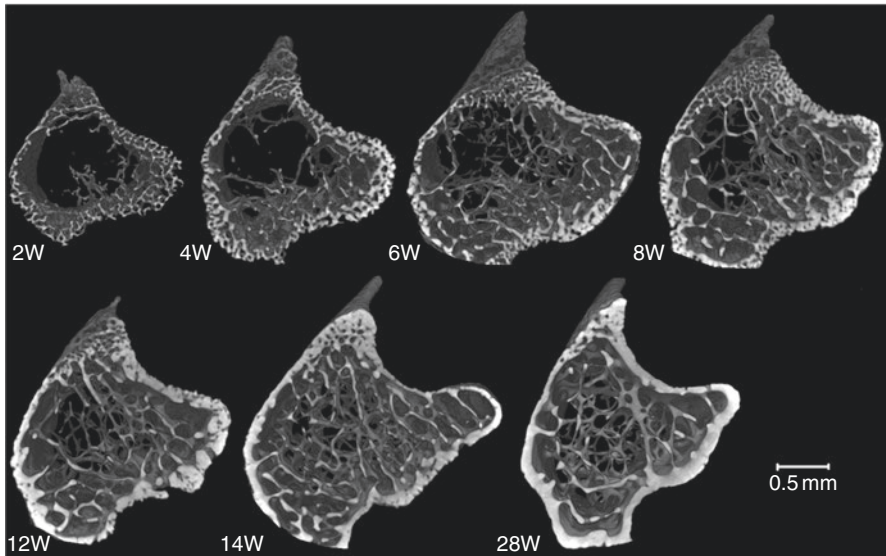
Fig. 18 Mouse bone growth with aging. W, weeks. Up to the age of 8 weeks, bone shape, trabecular bone, cortical bone structure, and bone mineral content tend to increase with age. At the ages of 8–12 weeks, the external shape of the bone becomes invariant, pores within the cortex are filled, and the cancellous bone becomes thicker

8   Summary

Osteoporosis significantly increases the risk of fracture. Once a fracture occurs, the bone shape becomes unstable and the risk of further fracture increases. It is desirable to monitor bone resorption, bone formation, and calcification to prevent fractures. The 4DQCT method can visualize calcified bone in three dimensions. There is a possibility that the resorption and formation of calcified bone can be estimated from the local bone change. In addition to bone density (BMD), bone morphology, and fracture strength, it is desirable to follow up on the therapeutic effect of osteoporosis.

MDCT can scan all parts of the body with minimal invasiveness, can identify the local fracture risk due to bone lesions, and can be applied to follow-up of diagnosis and treatment effects.

Table 2 Mouse bone growth with aging

	Weeks	2	4	6	8	12	14	28
1	Tt.Ar (mm²)	1.18 ± 0.04	1.78 ± 0.11	2.43 ± 0.05	2.37 ± 0.09	2.12 ± 0.11	2.45 ± 0.03	2.14 ± 0.13
2	Ct.Ar (mm²)	0.23 ± 0.01	0.52 ± 0.03	0.73 ± 0.05	0.80 ± 0.02	0.83 ± 0.01	0.86 ± 0.03	0.84 ± 0.02
3	BV (mm³)	0.016 ± 0.006	0.064 ± 0.016	0.159 ± 0.020	0.170 ± 0.033	0.109 ± 0.005	0.268 ± 0.031	0.112 ± 0.022
4	BV/TV (%)	1.51 ± 0.55	4.20 ± 0.70	7.56 ± 0.99	8.74 ± 1.33	6.78 ± 0.85	13.25 ± 1.40	6.87 ± 1.06
5	Tb.Th (μm)	26.00 ± 0.88	32.23 ± 1.64	31.94 ± 1.66	34.91 ± 1.10	35.90 ± 1.07	38.15 ± 1.16	41.47 ± 4.00
6	Tb.N (1/mm)	0.50 ± 0.16	0.97 ± 0.22	1.82 ± 0.30	1.90 ± 0.24	1.31 ± 0.09	2.56 ± 0.32	1.17 ± 0.16
7	Tb.Sp (μm)	293.23 ± 84.30	185.75 ± 29.35	180.09 ± 11.37	192.28 ± 24.16	199.99 ± 18.49	139.96 ± 11.58	180.64 ± 3.40
8	SMI	2.53 ± 0.14	2.53 ± 0.09	2.27 ± 0.22	2.30 ± 0.11	2.68 ± 0.14	2.22 ± 0.16	2.85 ± 0.19
9	V* m.space (mm³)	0.29 ± 0.01	0.27 ± 0.02	0.19 ± 0.02	0.15 ± 0.01	0.17 ± 0.03	0.07 ± 0.01	0.14 ± 0.02
10	V* tr (mm³)	0.0010 ± 0.0000	0.0020 ± 0.0003	0.0034 ± 0.0006	0.0035 ± 0.0007	0.0032 ± 0.0010	0.0051 ± 0.0003	0.0040 ± 0.0017
11	TB TMD (mg/cm³)	561.67 ± 3.31	581.20 ± 11.99	585.13 ± 24.52	619.50 ± 11.45	627.07 ± 6.20	628.60 ± 20.01	675.73 ± 20.28
12	CB TMD (mg/cm³)	667.40 ± 3.58	720.53 ± 15.00	758.13 ± 8.47	804.10 ± 9.13	879.70 ± 20.53	850.20 ± 38.88	933.27 ± 15.83

Tt.Ar, total cross-sectional area; Ct.Ar, cortical bone area; BV, bone volume; TV, total volume; Tb.Th, trabecular thickness; Tb.N, trabecular number; Tb.Sp, trabecular separation; SMI, structure model index; V* m.space, star volume of bone marrow space; V* tr, trabecular star volume TB, trabecular bone; CB, cortical bone; TMD, tissue mineral density

References

1. NIH. Osteoporosis prevention, diagnosis, and therapy. NIH Consens. Statement; 2000.
2. FDA. FDA Drug Safety Communication: Safety update for osteoporosis drugs, bisphosphonates, and atypical fractures; 2010.
3. Shane E, Burr D, Abrahamsen B, et al. Atypical subtrochanteric and diaphyseal femoral fractures: second report of a task force of the American society for bone and mineral research. J Bone Miner Res. 2014. https://doi.org/10.1002/jbmr.1998
4. Fields AJ, Lee GL, Liu XS, Jekir MG, Guo XE, Keaveny TM. Influence of vertical trabeculae on the compressive strength of the human vertebra. J Bone Miner Res. 2011. https://doi.org/10.1002/jbmr.207
5. Uda Y, Azab E, Sun N, Shi C, Pajevic PD. Osteocyte mechanobiology. Curr Osteoporos Rep. 2017. https://doi.org/10.1007/s11914-017-0373-0
6. Nango N, Kubota S, Hasegawa T, Yashiro W, Momose A, Matsuo K. Osteocyte-directed bone demineralization along canaliculi. Bone. 2016. https://doi.org/10.1016/j.bone.2015.12.006
7. Burr DB, Martin RB, Schaffler MB, Radin EL. Bone remodeling in response to in vivo fatigue microdamage. J Biomech. 1985. https://doi.org/10.1016/0021-9290(85)90204-0
8. Schaffler MB, Kennedy OD. Osteocyte signaling in bone. Curr Osteoporos Rep. 2012. https://doi.org/10.1007/s11914-012-0105-4
9. Wainwright SA, Biggs WD, Currey J, Gosline M. Mechanical design in organisms. Q Rev Biol. 1976;51:567.
10. Ito M, Ikeda K, Nishiguchi M, Shindo H, Uetani M, Hosoi T, Orimo H. Multi-detector row CT imaging of vertebral microstructure for evaluation of fracture risk. J Bone Miner Res. 2005. https://doi.org/10.1359/JBMR.050610.
11. Inamoto Y, Saitoh E, Okada S, et al. Anatomy of the larynx and pharynx: effects of age, gender and height revealed by multidetector computed tomography. J Oral Rehabil. 2015. https://doi.org/10.1111/joor.12298
12. Nango N, et al. Measurement of bone strength and medication evaluation can be achieved using medical CT images. Int Soc Bone Morphometry. 2015;13:43.
13. Bouxsein ML, Boyd SK, Christiansen BA, Guldberg RE, Jepsen KJ, Müller R. Guidelines for assessment of bone microstructure in rodents using micro-computed tomography. J Bone Miner Res. 2010. https://doi.org/10.1002/jbmr.141
14. Endo N, Yamamoto T et al (2014) Moden bone Histomorphometry.
15. Amstrup AK, Jakobsen NFB, Lomholt S, Sikjaer T, Mosekilde L, Rejnmark L. Inverse correlation at the hip between areal bone mineral density measured by dual-energy X-ray absorptiometry and cortical volumetric bone mineral density measured by quantitative computed tomography. J Clin Densitom. 2016;19:226–33.
16. Inoue K, Hamano T, Nango N, et al. Multidetector-row computed tomography is useful to evaluate the therapeutic effects of bisphosphonates in glucocorticoid-induced osteoporosis. J Bone Miner Metab. 2014. https://doi.org/10.1007/s00774-013-0485-2
17. Hildebrand T, Rüegsegger P. A new method for the model-independent assessment of thickness in three-dimensional images. J Microsc. 1997. https://doi.org/10.1046/j.1365-2818.1997.1340694.x
18. Hildebrand T, Rüegsegger P. Quantification of bone microarchitecture with the structure model index. Comput Methods Biomech Biomed Engin. 1997. https://doi.org/10.1080/01495739708936692
19. Vesterby A, Gundersen HJG, Melsen F. Star volume of marrow space and trabeculae of the first lumbar vertebra: sampling efficiency and biological variation. Bone. 1989. https://doi.org/10.1016/8756-3282(89)90140-3
20. Carte DR, Hayes WC. The compressive behavior of bone as a two-phase porous structure. J Bone Jt Surg – Ser A. 1977. https://doi.org/10.2106/00004623-197759070-00021
21. Sharir A, Stern T, Rot C, Shahar R, Zelzer E. Muscle force regulates bone shaping for optimal loadbearing capacity during embryogenesis. Development. 2011. https://doi.org/10.1242/dev.063768